6-1-2010

Modeling radiation belt radial diffusion in ULF wave fields: 1. Quantifying ULF wave power at geosynchronous orbit in observations and in global MHD model

Chia-Lin L. Huang
hcl@guero.sr.unh.edu

Harlan E. Spence
University of New Hampshire, harlan.spence@unh.edu

Howard J. Singer

W. Jeffrey Hughes

Recommended Citation

Huang, C.-L., H. E. Spence, H. J. Singer, and W. J. Hughes (2010), Modeling radiation belt radial diffusion in ULF wave fields: 1. Quantifying ULF wave power at geosynchronous orbit in observations and in global MHD model, J. Geophys. Res., 115, A06215, doi:10.1029/2009JA014917.

JOURNAL OF GEOPHYSICAL RESEARCH, VOL. 115, A06215, doi:10.1029/2009JA014917, 2010

Modeling radiation belt radial diffusion in ULF wave fields: 1. Quantifying ULF wave power at geosynchronous orbit in observations and in global MHD model

Chia-Lin Huang,[1] Harlan E. Spence,[1,2] Howard J. Singer,[3] and W. Jeffrey Hughes[1]

Received 21 September 2009; revised 6 January 2010; accepted 3 February 2010; published 25 June 2010.

[1] To provide critical ULF wave field information for radial diffusion studies in the radiation belts, we quantify ULF wave power (f = 0.5–8.3 mHz) in GOES observations and magnetic field predictions from a global magnetospheric model. A statistical study of 9 years of GOES data reveals the wave local time distribution and power at geosynchronous orbit in field-aligned coordinates as functions of wave frequency, solar wind conditions (V_x, ΔP_d and IMF B_z) and geomagnetic activity levels (*Kp*, *Dst* and *AE*). ULF wave power grows monotonically with increasing solar wind V_x, dynamic pressure variations ΔP_d and geomagnetic indices in a highly correlated way. During intervals of northward and southward IMF B_z, wave activity concentrates on the dayside and nightside sectors, respectively, due to different wave generation mechanisms in primarily open and closed magnetospheric configurations. Since global magnetospheric models have recently been used to trace particles in radiation belt studies, it is important to quantify the wave predictions of these models at frequencies relevant to electron dynamics (mHz range). Using 27 days of real interplanetary conditions as model inputs, we examine the ULF wave predictions modeled by the Lyon-Fedder-Mobarry magnetohydrodynamic code. The LFM code does well at reproducing, in a statistical sense, the ULF waves observed by GOES. This suggests that the LFM code is capable of modeling variability in the magnetosphere on ULF time scales during typical conditions. The code provides a long-missing wave field model needed to quantify the interaction of radiation belt electrons with realistic, global ULF waves throughout the inner magnetosphere.

Citation: Huang, C.-L., H. E. Spence, H. J. Singer, and W. J. Hughes (2010), Modeling radiation belt radial diffusion in ULF wave fields: 1. Quantifying ULF wave power at geosynchronous orbit in observations and in global MHD model, *J. Geophys. Res.*, *115*, A06215, doi:10.1029/2009JA014917.

1. Introduction

[2] Among the proposed mechanisms that control radiation belt dynamics, large amplitude ULF pulsations have the potential to supply the energy necessary to create variability in the relativistic electron fluxes [*Hudson et al.*, 1999, 2000; *Elkington et al.*, 1999, 2003]. If global magnetohydrodynamic (MHD) codes are able to reproduce ULF waves, following relativistic electrons in the MHD fields would then allow us to understand the behavior of radiation belt electrons in ULF wave fields. The broad goal of this paper (and the companion paper [*Huang et al.*, 2010]) is to determine the radial diffusion rate of radiation belt electrons through computer simulations. In this paper, we characterize the major features of the ULF wave fields during various solar wind conditions and geomagnetic activity levels using geosynchronous observations and a global magnetospheric model. Under circumstances when the global MHD code works well, we can simulate the radiation belt electrons in electric and magnetic fields that represent a realistic, dynamic magnetosphere. In the companion paper [*Huang et al.*, 2010], we determine the rate of radial transport of radiation belt electrons at the equatorial plane using a global MHD code and a particle tracing code.

[3] There is an extensive and rich literature on ultralow frequency (ULF) oscillation research [*Takahashi et al.*, 2006, and references therein]. While questions still exist about the sources and propagation of ULF waves, that is not the aim of our study. Rather, the focus of this paper is to quantify specifically those characteristics of ULF wave power necessary to better understand their effects on radiation belt electrons. ULF waves are thought to play an important role in the transport and acceleration of energetic particles in the magnetosphere and are among the proposed mechanisms that control the variability of radiation belt electrons. Recent statistical studies find a strong correlation between ULF wave power and outer zone electron flux [*Rostoker et al.*, 1998;

[1]Center for Space Physics, Boston University, Boston, Massachusetts, USA.
[2]Also at Institute for the Study of Earth, Oceans, and Space, University of New Hampshire, Durham, New Hampshire.
[3]Space Weather Prediction Center, NOAA, Boulder, Colorado, USA.

0148-0227/10/2009JA014917

O'Brien et al., 2001]. In addition, *Hudson et al.* [1999] and *Elkington et al.* [1999] suggest that large amplitude ULF pulsations could supply the energy necessary to generate variability in the relativistic electron flux. Therefore, quantifying the spatial distribution and amplitude of ULF waves in the magnetosphere for different solar wind conditions is essential for better understanding these wave-particle interactions in the radiation belt environment.

[4] *Dungey* [1954] first proposed that these long-lasting periodic geomagnetic oscillations might be the signature of standing Alfvén waves being excited on magnetic field lines. Different classes of magnetospheric pulsations have different sources. In general, ULF waves are associated with low-frequency plasma waves that arise due to perturbations of magnetic flux tubes. Primary sources of magnetospheric ULF waves are solar wind variations in dynamic pressure and IMF B_z, bounce and drift resonances with ring current ions, substorm injections, cavity mode excitations and the Kelvin-Helmholtz instability at the magnetopause [*Pu and Kivelson*, 1983; *Hughes*, 1994]. These different mechanisms perturb the magnetosphere on large scales and generate ULF waves with different spatial distributions, frequency ranges, and harmonic structures.

[5] ULF wave surveys have been carried out both from ground observations and measurements in space. Ground-based observations are excellent for studying ULF waves because they provide continuous coverage over a large portion of Earth's surface. However, the signals measured on the ground are mostly the transverse components and the low-mode number waves that propagate through the ionosphere. Spacecraft observations provide in situ measurements, which have greatly enhanced our understanding of ULF waves. Based on field measurements from GOES, CRRES, AMPTE, and ISEE satellites, statistical studies provide wave occurrence rates and integrated wave power from the near-Earth region to the magnetopause location [e.g., *Higuchi and Kokubun*, 1988; *Anderson et al.*, 1990; *Zhu and Kivelson*, 1991; *Hudson et al.*, 2004; *Brautigam et al.*, 2005]. For example, *Zhu and Kivelson* [1991] showed the spatial distribution of mean wave amplitude for the compressional, azimuthal and radial components of magnetic field fluctuations using ISEE-1 and 2. They showed that intense compressional ULF waves are strong near the flanks of the magnetosphere and azimuthal waves peak on the nightside. A number of excellent reviews of geomagnetic pulsations are available which provide extensive background of the subject, e.g., *Southwood and Hughes* [1983] and *Anderson* [1994].

[6] Even though ULF waves have been studied for several decades, comprehensive statistical maps of global, time-dependent, geomagnetic wave activity that can provide the crucial element for a quantitative understanding of drift-averaged wave-particle interactions do not exist. Theoretically, global magnetohydrodynamic (MHD) codes are capable of reproducing MHD waves, such as ULF waves. However, to date, the only ULF wave analysis from a global MHD code are by *Elkington et al.* [2004] and *Claudepierre et al.* [2008] and S. Claudepierre, M. Hudson, W. Lotko, J. Lyon, and R. Denton (Solar wind driven of magnetospheric ULF waves: Field line resonances driven by dynamic pressure fluctuations, submitted to *Journal of Geophysical Research*, 2010). *Elkington et al.* [2004] found that the power spectral density (PSD) of ULF waves at local dusk in the Lyon-Fedder-Mobarry (LFM) global MHD code [*Lyon et al.*, 2004] during a geomagnetic storm sharply decreases toward the inner regions of the magnetosphere, in good agreement with average ground-based observations. *Claudepierre et al.* [2008] show surface waves near the flanks in the LFM code which are generated by the Kelvin-Helmholtz instability. S. Claudepierre et al. (submitted, 2010) used the LFM code to investigate how the solar wind dynamic pressure fluctuations drive field line resonances on the dayside magnetosphere. Nevertheless, further investigation and validation are needed to better quantify wave characteristics in global MHD codes for the benefit of studying wave-particle interactions using combined global MHD code and particle tracing code [*Hudson et al.*, 1999; *Elkington et al.*, 2003, 2004].

[7] Geosynchronous orbit is located conveniently in the outer electron belt, and provides many magnetic field and particle measurements. Therefore, geosynchronous orbit is an ideal place for assessing ULF wave properties to better understand the behavior of relativistic electrons in global ULF wave fields. In this study, we use 9 years of GOES magnetic field data to characterize the local time distribution and wave amplitude of ULF waves at geosynchronous orbit during various solar wind conditions and geomagnetic activity levels. While previous studies derive the integrated wave power and occurrence rate of ULF waves, we calculate the power spectral density as a function of frequency to provide the appropriate wave characteristics for electrons of different energies and hence different resonant drift periods. In addition, in order to understand the dynamic behavior of radiation belt electrons in realistic ULF wave fields, a global, self-consistent, and time-dependent magnetospheric model is needed. Therefore, we compare the power spectral density of GOES data with the simulation results of the LFM code, to examine the ability of one global magnetospheric model to reproduce wave features statistically.

2. ULF Wave Spectra at Geosynchronous Orbit

2.1. GOES Magnetic Field Data

[8] The GOES statistical study uses 9 years (1995–2003) of magnetic field data from GOES-8, 9 and 10 satellites with 1 min time resolution. Durations of the satellite data used in this study are as follows: GOES-8 (1995/12/1–2003/4/8); GOES-9 (1995/12/1–1998/7/27); and GOES-10 (1999/3/1–2003/12/31). To separate compressional and transverse waves in the magnetic field data, we rotate the data into magnetic field-aligned coordinates (FAC). FAC axes are defined with $\boldsymbol{b}$ parallel to an 1 h running average of the magnetic field direction, $\boldsymbol{\phi}$ parallel to the vector product of the $\boldsymbol{b}$ vector and the spacecraft geocentric position vector and positive eastward, and $\boldsymbol{n}$ completing the triad. The parallel component B_b contains most of the field magnitude and shows the known, strong diurnal variation at geosynchronous orbit. B_ϕ (azimuthal) and B_n (radial) are the transverse components of the field, which fluctuate with zero mean. Variations of B_b and $|B|$ are compressional waves; and fluctuations in B_ϕ and B_n are the toroidal and poloidal modes, respectively. The variations in the $\boldsymbol{b}$ component are stronger than the other two components and generate most of the electric fields in the azimuthal direction, according to Faraday's law. Electrons executing azimuthal gradient and curvature drift in the radiation belt will undergo the greatest acceleration when the electric field

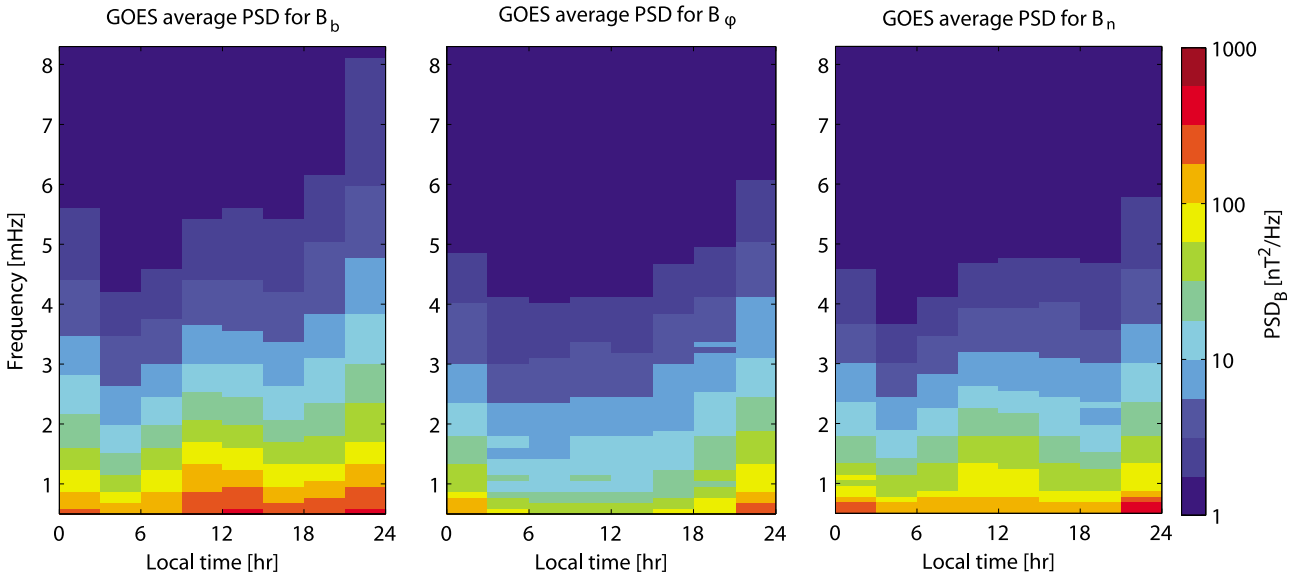

Figure 1. Average PSDs of GOES data in magnetic field-aligned coordinates. (left) B_b, the parallel component; (middle) B_ϕ, the azimuthal component; and (right) B_n, the radial component. Wave power as a function of local time and frequency is shown on a colored logarithmic scale from 10^0 to 10^3 nT^2/Hz. The wave power peaks in the noon and midnight sectors for the compressional component and peaks on the nightside for the azimuthal and radial components. In each local time bin, there are >7500 PSD samples of 3 h intervals of GOES data.

points in the direction of the electron drift path. Therefore, electric fields in the azimuthal direction are believed to have the largest effect on radiation belt electrons [*Elkington et al.*, 2003].

[9] To better understand the local time distribution of ULF waves, we divide the magnetic field data into eight 3 h local time sectors starting from local midnight. GOES-8 is at local midnight at 0500 UT, so the GOES-8 data are divided into intervals 0500–0800 UT, 0800–1100 UT, etc. GOES-9 and 10 pass local midnight at 0900 UT, so the corresponding intervals are 0900–1200 UT, 1200–1500 UT, etc. As a result, daily GOES data are separated into eight local time sectors starting from local midnight. We then calculate the power spectral density within each 3 h interval to explore the average wave power and local time distribution at geosynchronous orbit.

[10] Power spectral density (PSD) is a parameter used to reveal the underlying periodicity in data, especially for time series data. To calculate PSD, we (1) exclude intervals that have a sudden or discontinuous change in the time series data (e.g., magnetopause crossings or data gaps); (2) detrend the data with a 3rd degree polynomial fit to eliminate slow variations caused by the diurnal variation of the magnetic field at geosynchronous orbit; (3) despike data points which exceed three standard deviations; (4) run a high pass filter to attenuate frequencies lower than some desired cutoff frequency (0.5 mHz is the lower limit of ULF waves considered in this study); and (5) perform a Fast Fourier Transform to obtain the PSD in units of nT^2/Hz.

2.2. Average PSD in Parallel and Transverse Components

[11] We repeat the procedure to calculate PSD of the 3 h GOES data of all three field components in FAC. The Nyquist frequency of the 1 min GOES data is 8.3 mHz. The total number of 3 h GOES intervals is greater than 60000, with >7500 PSD samples in each local time sector. Variations among the PSDs are large, spanning 4 orders of magnitude between the maximum and minimum values. To demonstrate the general wave characteristics, we show only the median value of the PSDs in each frequency bin and call it the "average PSD." However, it is important to stress that individual events rarely exhibit the exact spectral features of the average PSD.

[12] Figure 1 illustrates the average PSD of GOES data at all local times for the three FAC components. In each panel, the X axis is the satellite local time in hours, and the Y axis is wave frequency in mHz with the Nyquist frequency of 8.3 mHz. The color pixels show the wave power for each frequency and local time bin in units of nT^2/Hz. The wave power in all field components decreases with increasing frequency rapidlly at all local times. The local time distribution of the compressional component (B_b) peaks in the noon and midnight sectors. The noon peak is likely driven by solar wind dynamic pressure that perturbs the dayside magnetopause at ULF wave frequencies [*Kepko et al.*, 2002]. Geostationary orbit is closest to the magnetopause at noon, so the ULF waves generated by solar wind pressure variations peak at noon in the GOES data. The midnight peak, slightly toward the premidnight sector, is likely the consequence of storm or substorm activity driven by strong tail dynamics (i.e., substorm injections, flow braking etc.). The azimuthal and radial component power (B_ϕ and B_n) peaks on the nightside with less wave power than the compressional component. The average PSD for B_ϕ is likely lower than the other two components on the dayside. This could be because the field line resonance has a node at magnetic equator for the fundamental toroidal mode which makes it difficult for

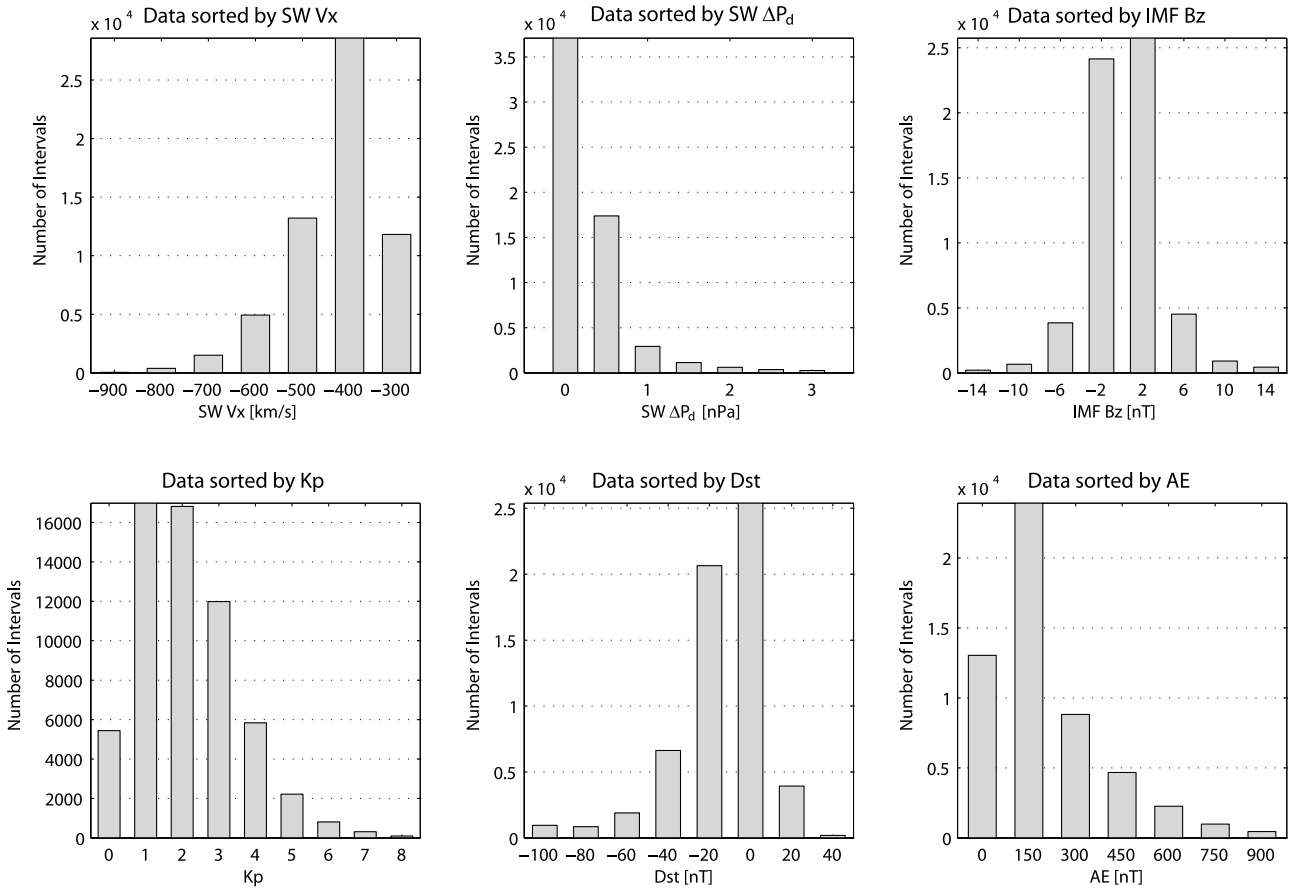

Figure 2. Number of 3 h intervals of GOES data sorted by (top) solar wind velocity V_x, dynamic pressure variations ΔP_d, and IMF B_z, and (bottom) geomagnetic indices *Kp*, *Dst*, and *AE*. We select the parameter bins in such way that >98% of the GOES data are included.

low-inclination satellites, like GOES (5 to 10 degrees off the magnetic equator), to measure this type of fluctuation [*Singer and Kivelson*, 1979]. To clarify how the ULF waves are distributed in local time and wave amplitude for different magnetospheric states, we next explore the wave characteristics at geosynchronous orbit during various solar wind conditions and geomagnetic activity levels.

2.3. ULF Waves at GEO as Functions of Given Parameters

[13] It is necessary to find a good sorting parameter for ULF waves to simplify the calculation of radial diffusion coefficients. Historically, *Kp* is commonly used as the ULF wave power indicator for estimation of radial diffusion coefficients [*Brautigam and Albert*, 2000]. In this study, 3 h GOES data are sorted by parameters that represent the solar wind drivers and magnetospheric perturbations, such as the solar wind velocity V_x, dynamic pressure variations ΔP_d (standard deviation of 3 h pressure data), IMF B_z, *Kp*, *Dst*, and *AE* indices. We sort the data based on the median value of each parameter during the 3 h interval. The solar wind and IMF data are obtained from the Wind satellite and are propagated ballistically to Earth's location. The geomagnetic indices are obtained from Geomagnetic Data Service at Kyoto (the *AE* index is unavailable for 1995 and 1996).

[14] Figure 2 shows number of the 3 h GOES intervals sorted by each parameter. We select the parameter bins in such a way that >98% of the data are included in this analysis. The minimum in each bin is 400 samples (i.e., 400 independent 3 h intervals). When sorting data by solar wind V_x, we use parameter bins centered at −300, −400, −500, −600, −700, −800, and −900 km/s. Data in each bin contain solar wind V_x within ±50 km/s (half of the bin size) of these central values. Similarly, the dynamic pressure variation bins for the 3 h data are center at 0, 0.5, 1, 1.5, 2, 2.5, and 3 nPa; the IMF B_z bins are centered at −14, −10, −6, −2, 2, 6, 10, and 14 nT; the *Kp* bins contain values from 0 to 8; the *Dst* bins are centered at −100, −80, −60, −40, −20, 0, 20, and 40 nT; and the *AE* bins are centered at 0, 150, 300, 450, 600, 750, and 900 nT.

[15] According to the solar wind V_x histogram, the most probable solar wind velocity in this survey is $V_x = -400$ km/s, and the histogram drops steeply as velocity increases or decreases away from this value. Similar to solar wind velocity, the pressure variation ΔP_d histogram peaks at low values (<1 nPa) and drops rapidly as the increase of pressure variations. The IMF B_z histogram is symmetric about 0 nT. It is worth pointing out that even with an average B_z of +2 nT or higher, there could still be intervals of B_z southward during any 3 h interval. The magnetospheric activity level is generally moderate as shown by the histograms of geomagnetic

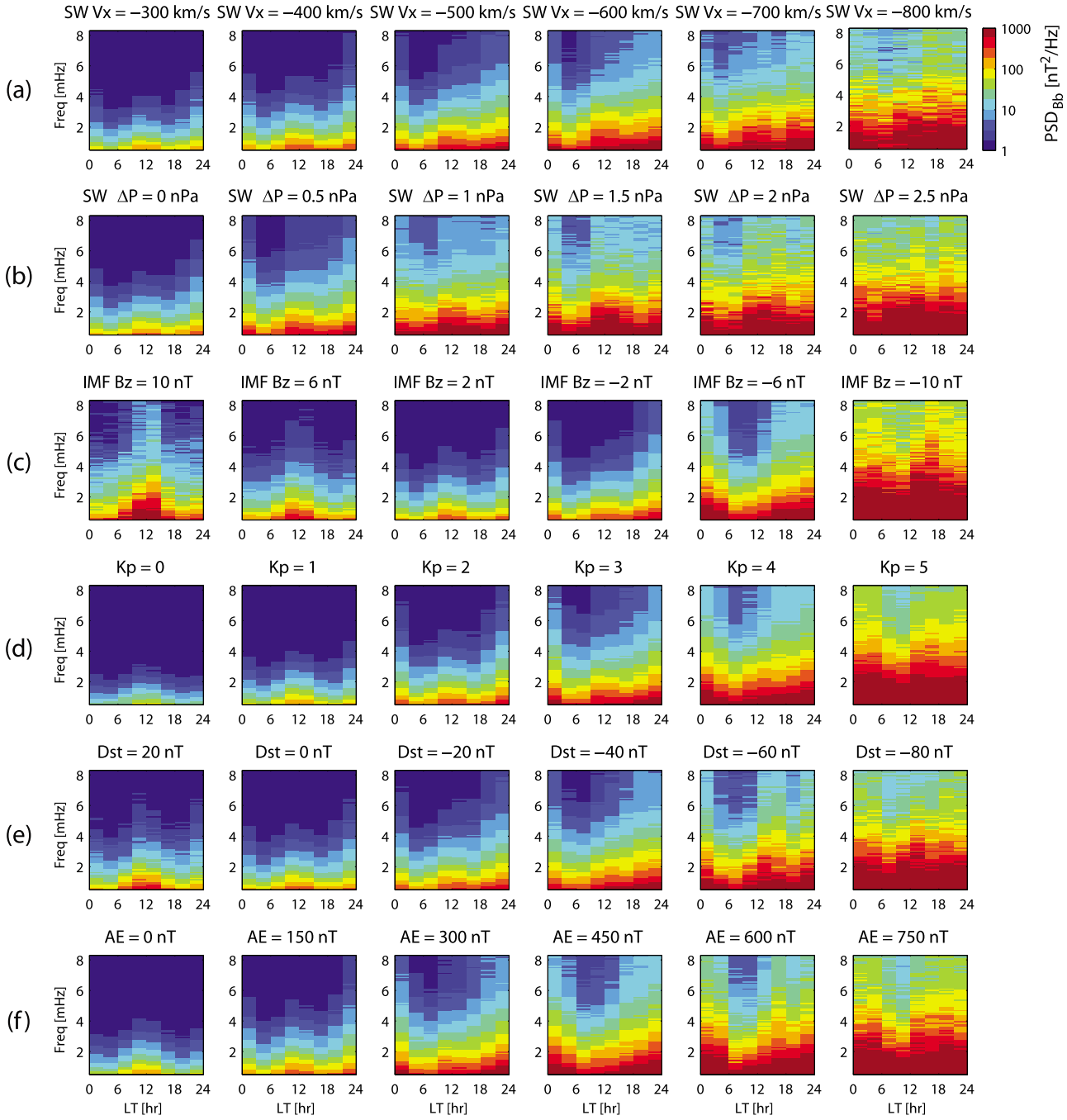

Figure 3. GOES B_b PSDs sorted by (a) solar wind V_x, (b) dynamic pressure variations ΔP_d, (c) IMF B_z, (d) Kp, (e) Dst, and (f) AE. ULF wave power as a function of local time and frequency is shown on a colored logarithmic scale from 10^0 to 10^3 nT^2/Hz.

indices. These parameter distributions are expected from earlier studies which confirms that our sampling is representative of the typical broad range of states of solar wind conditions and geomagnetic responses. To quantify ULF wave properties during different states of the magnetosphere, we investigate the average GOES PSDs as functions of the six parameters discussed above.

[16] The PSDs of GOES data as functions of solar wind V_x, dynamic pressure variations ΔP_d, IMF B_z, Kp, Dst and AE are shown in rows from top to bottom in Figures 3, 4, and 5 for B_b, B_ϕ, and B_n components, respectively. Each panel is the average PSD within the range of the selected parameter. The color pixels are the wave power of each local time and frequency bin using the same logarithmic scale from 10^0 to 10^3 nT^2/Hz. When the number of samples in the bins is high, the average PSDs across the frequencies are relatively smooth (e.g., $V_x = -400$ km/s). On the other hand, the average PSDs across frequency bins are noisy when the sample rate is lower (e.g., $V_x = -800$ km/s).

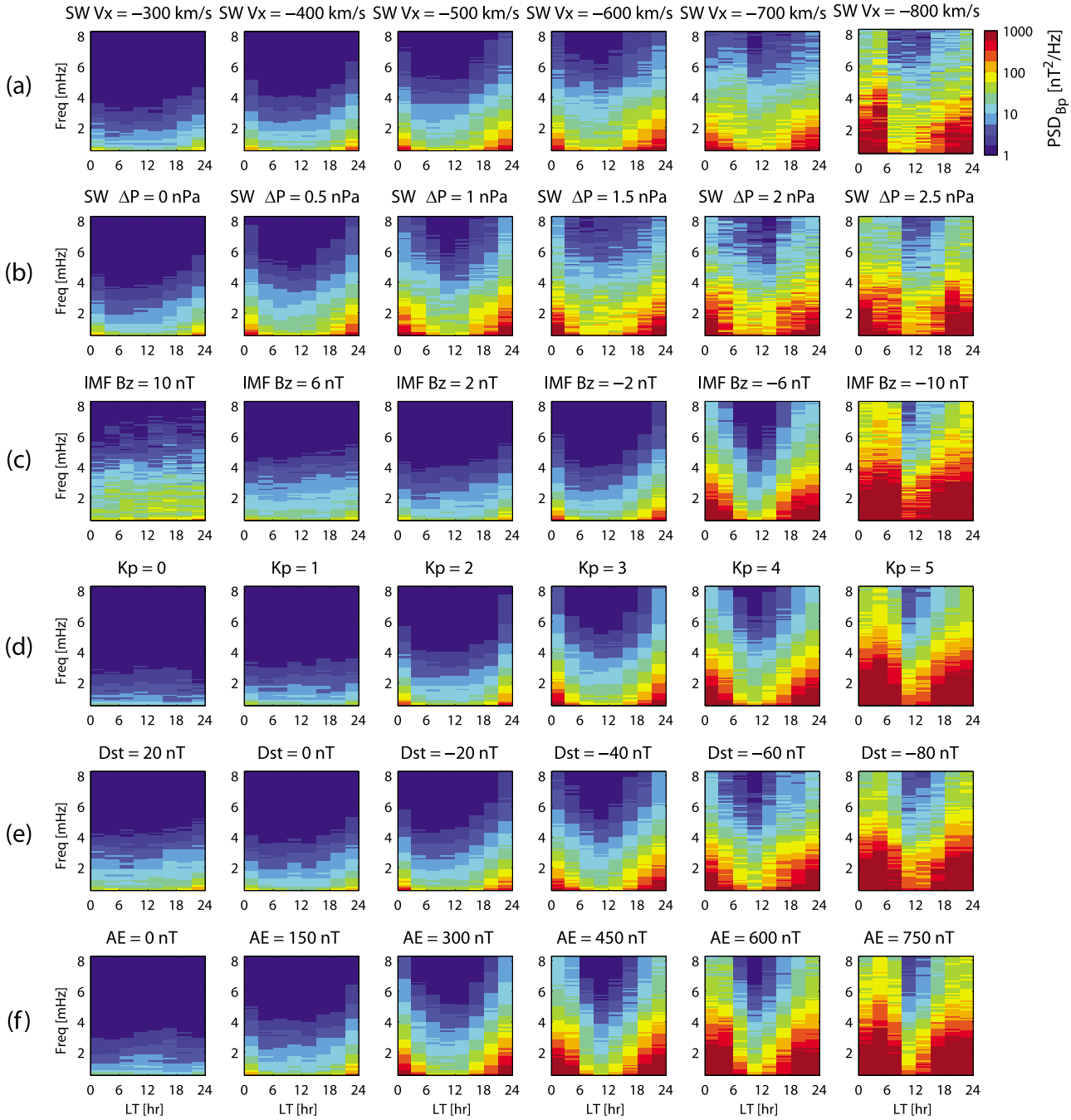

Figure 4. GOES B_ϕ PSDs sorted by (a) solar wind V_x, (b)dynamic pressure variations ΔP_d, (c) IMF B_z, (d) *Kp*, (e) *Dst*, and (f) *AE*. ULF wave power as a function of local time and frequency is shown on a colored logarithmic scale from 10^0 to 10^3 nT^2/Hz.

[17] The local time dependence for each component is clearly shown in Figures 3, 4, and 5, especially in the higher solar wind condition and geomagnetic activity bins. In general, the increase of ULF wave power in the compressional, azimuthal and radial components varies similarly as the level of each parameter increases. We discuss the general variations of wave power as functions of selected parameters below in detail.

[18] Solar wind velocity is one of the most frequently used parameters for sorting levels of ULF wave power in magnetospheric studies, [e.g., *Mathie and Mann*, 2001]. As shown in Figures 3a, 4a, and 5a, the wave power at all local times and frequencies increases monotonically as solar wind V_x increases. Similar to solar wind velocity, the GOES wave power as a function of dynamic pressure variations ΔP_d also increases monotonically as shown in Figures 3b, 4b, and 5b. Generally, variations in solar wind dynamic pressure are larger during periods of higher solar wind velocity, which generates more wave activity on the dayside magnetosphere. In addition, higher solar wind velocity (and hence velocity

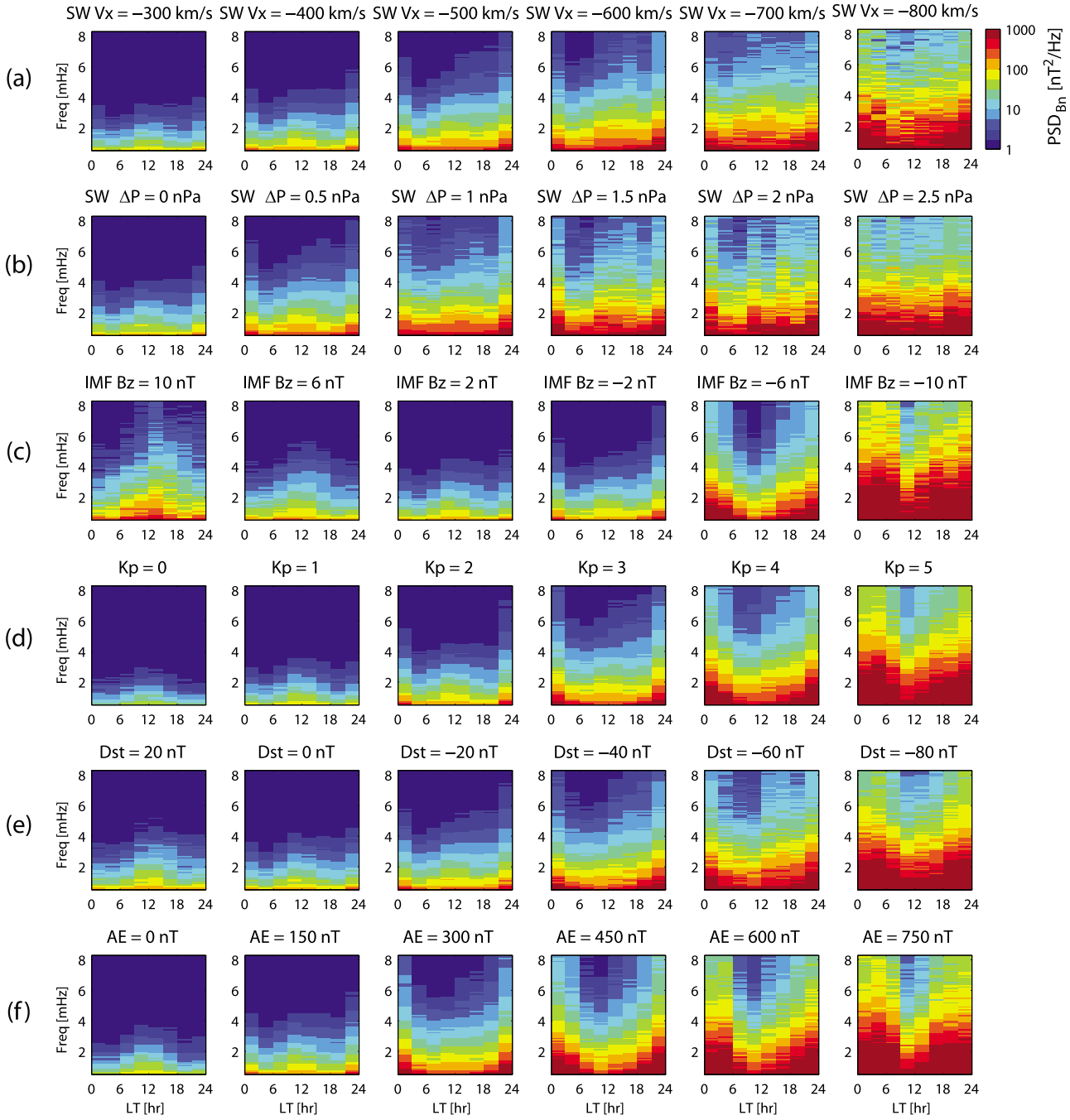

Figure 5. GOES B_n PSDs sorted by (a) solar wind V_x, (b) dynamic pressure variations ΔP_d, (c) IMF B_z, (d) *Kp*, (e) *Dst*, and (f) *AE*. ULF wave power as a function of local time and frequency is shown on a colored logarithmic scale from 10^0 to 10^3 nT^2/Hz.

shear) is effective for exciting the Kelvin-Helmholtz instability at the flanks [*Pu and Kivelson*, 1983]. However, high solar wind velocity intervals are usually complicated. In particular, they can be associated with strong IMF southward events which have different effects on wave power and distribution in the magnetosphere.

[19] Figures 3c, 4c, and 5c show the differences in wave properties between generally open and closed magnetospheric configurations by sorting the PSDs by IMF B_z. During periods of IMF B_z northward, wave power maxima are concentrated on the dayside and are likely dominated by the direct driving of compressional waves by solar wind pressure variations. For the large positive B_z intervals ($B_z = 10$ nT), the strong dayside wave power is probably dominated by sudden storm commencements or magnetic cloud sheath impacts with high density variations. Throughout IMF B_z southward intervals, the coupling processes between the solar wind and magnetosphere create stronger and more global perturbations in the magnetosphere than during northward IMF intervals. For example, the field dipolarization pro-

cess during substorm events enhances the wave power in the nightside magnetosphere. During magnetic storms, with long intervals of southward IMF, the global disturbances expand and intensify the wave activity at geosynchronous orbit to all local times.

[20] The geomagnetic indices, *Kp*, *Dst* and *AE*, represent the levels of magnetospheric activity globally, in the ring current and in the auroral regions, respectively. *Kp* indicates the average global field disturbances measured from a number of midlatitude ground magnetometers distributed around the world. *Dst* is the average magnetic depression near the equator resulting from the formation of the ring current during magnetic storms. *AE* measures the horizontal auroral electrojet current which is related to the intensity of substorm activity and magnetospheric convection.

[21] The ULF wave power increases monotonically as the global disturbance intensifies, similar to the wave characteristics sorted by solar wind V_x. Figures 3d, 3e, 4d, 4e, 5d, and 5e show that the wave power as a function of *Kp* and *Dst* grows at all local times, because these indices describe field perturbations on a global scale. The *AE*-dependent wave properties show a preference for the nightside, shown in Figures 3f, 4f, and 5f, as a result of substorm dynamics and magnetospheric convection which favor the midnight sector, including the tail field dipolarization during substorm events. *Kp* is one of the commonly used parameters for sorting ULF wave power, [e.g., *Takahashi and Anderson*, 1992]. *Takahashi and Anderson* [1992] use AMPTE CCE magnetic field data to investigate the distribution of ULF energy in Pc3-4 bands ($f < 80$ mHz), which shows similar local time and *Kp* dependence to our study (~Pc5 band). In all given parameters, there is a dawn-dusk asymmetry in the ULF wave power during higher magnetospheric activity, especially in the azimuthal and radial components. The generally accepted view is that the dawn-dusk asymmetry is due to the westward drift path of ions which results in unstable ring current ion distributions in the dusk sector [*Southwood*, 1977; *Hughes et al.*, 1978; *Wilson et al.*, 2006].

[22] Figures 3, 4, and 5 represent the most comprehensive observational ULF wave study at geosynchronous orbit using the largest GOES data set. Figures 3, 4, and 5 reveal the power spectral density and local time distribution of ULF waves under different conditions and circumstances that is targeted toward the outer zone electron studies. This is also valuable for constructing an empirical wave field model based on observations for different solar wind inputs or geomagnetic activity levels. For example, GOES ULF wave data can be expressed in polynomial equations as shown in Figure 6. In this case, for simplicity, we do not consider the local time information because electron drift periods are much shorter than diffusion time scales. The local time averaged PSDs are shown using a logarithmic scale with different color dots representing values from different solar wind V_x and geomagnetic activity *Kp* bins. The gray curves are 3rd degree polynomial fits to the PSD sets in the least-square sense. Based on GOES data, the polynomial equation of ULF wave power at geosynchronous orbit is:

$$P(f) = C_3 f^3 + C_2 f^2 + C_1 f + C_0 \quad (1)$$

in units of [nT^2/mHz] in logarithmic scale. The coefficients C_3, C_2, C_1, and C_0 for different solar wind V_x and *Kp* levels for B_b, B_ϕ, and B_n components are listed in Table 1. One can generate analytical ULF wave fields based on this equation to simulate radial transport of radiation belt electrons in the manner of *Perry et al.* [2006]. Next, we use the same technique and data set to quantify statistically the wave characteristics in a global magnetospheric MHD code.

3. Statistical Comparisons of Data and Model

[23] In the reference by *Huang et al.* [2006], the capabilities of the LFM MHD code to predict the ambient magnetic field were examined by statistical comparisons with GOES data. Quantitative statistical studies of the MHD simulations show that MHD field lines are consistently under-stretched, especially during storm time ($Dst < -20$ nT) on the nightside, a likely consequence of an insufficient representation of the inner magnetosphere current systems in ideal MHD at the LFM grid resolution we used. However, the LFM code makes reasonable predictions of magnetic fields at geosynchronous orbit during nonstorm time intervals ($Dst > -20$ nT). *Huang et al.* [2006] examined the predictive capability of the models for the field configuration and magnitude for long-term, average trends on the scale of hours and days. In this study, the model outputs are compared with GOES data on a much shorter time scale (minutes) to test the performance of the MHD code for predicting magnetospheric pulsations in the ULF wave frequency range.

[24] Using the LFM code, we simulate 27 days taken from the interval 23 February to 26 April 1996, and statistically compare the model results with GOES-8 PSD data in the same time interval. The time resolution of this LFM simulation was chosen to be 2 minutes, a balance between sufficient time resolution for ULF study and reasonable data storage. The Nyquist frequency of the model and data comparisons is thus 4.2 mHz. The spatial resolution of the LFM code at geosynchronous orbit is between 0.25 and 0.5 R_E, which is adequate to capture ULF waves. The solar wind is the plasma source in the LFM code. The code does not include ion outflow from an ionosphere or plasmasphere model, so the number density in the inner magnetosphere of the simulations is lower than what is typically observed. We use the solar wind and IMF data (1 min) measured by the Wind satellite downloaded from CDAWeb as the upstream boundary conditions to drive the LFM code. The 27 days simulation is not continuous due to perigee passes of the Wind satellite. However, this time interval represents typical solar wind conditions including long quiet periods, periods of moderate geomagnetic activity ($Dst > -50$ nT) and several substorm events. The range of the solar wind data covered in the 27 d interval is described as the median values and standard deviations of three representative parameters: solar wind velocity V_x (397 ± 77 km/s), proton number density (7.1 ± 5.5 cm^{-3}), and IMF B_z (−0.5 ± 2.5 nT).

[25] To quantify ULF wave predictions in the LFM code, we calculate the power spectral density for each 3 h interval of the 27 days. Since these global models were developed to describe the large-scale configurations and dynamics of the magnetosphere, it is not surprising that the model wave predictions for individual events are poor. To compare the statistical properties of ULF waves in the data and model outputs, we take the median PSD values in each frequency bin to obtain the average PSD for all local time sectors and field

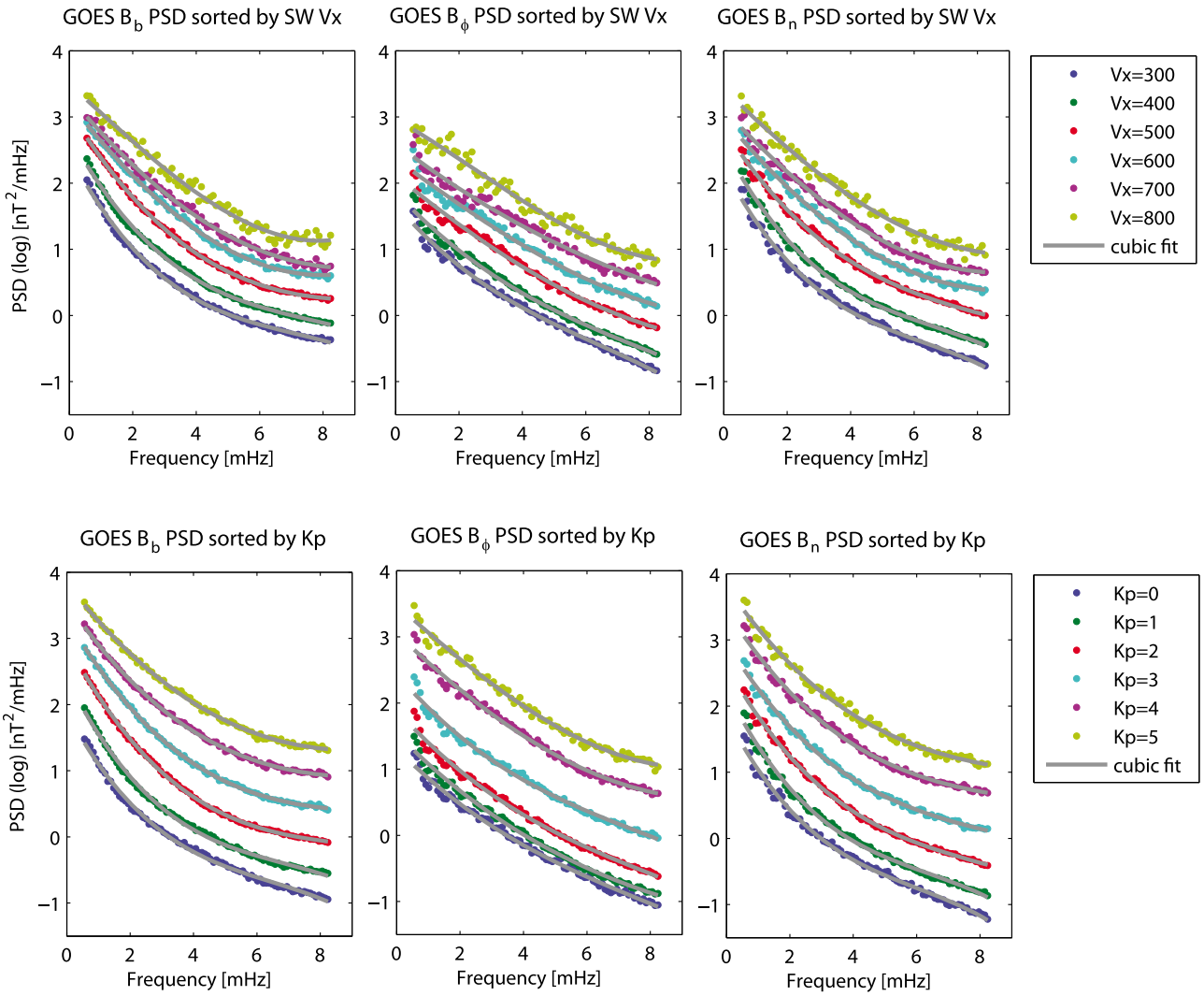

Figure 6. Local time averaged PSDs of GOES (left) B_b, (middle) B_ϕ, and (right) B_n components sorted by solar wind (top) *Vx* and (bottom) *Kp*. The gray lines show the cubic fit of GOES PSDs in each *Vx* and *Kp* bins. The fitting coefficients are listed in Table 1.

components. We then compare the average PSDs of GOES data and the LFM outputs for the same 27 d interval statistically in Figure 7. In each part, the color pixels show the PSD values of vector magnetic field versus local time and frequency with the same logarithmic scale. Figure 7 (top) is the ULF wave power calculated from GOES-8 data, and Figure 7 (bottom) is from the LFM model results.

[26] For the zeroth order, the LFM code predicts ULF wave power well for all field components when compared statistically to GOES data. In the B_b component, LFM generates higher power on the dayside and lower power on the nightside than the GOES observations. For the B_ϕ component, LFM predicts very similar ULF wave power compared to the observations in all frequencies and local time sectors. Finally, LFM overestimates the higher frequency range in most local times when compared to GOES data. Although the LFM nightside field configurations are under-stretched in most conditions [*Huang et al.*, 2006], the code reproduces wave activity on the nightside during this time interval reasonably well, especially in the perpendicular components.

[27] ULF wave power observed at geosynchronous is very sensitive and highly variable, spanning 4 orders of magnitude between maximum and minimum wave powers. Therefore, it is difficult to reproduce quantitatively the exact ULF wave powers as the observations using a global MHD code. Nevertheless, LFM gives a reasonable qualitative wave power distribution in local time and frequency during a 27 day nonstorm interval and shows its capability of modeling variations in the magnetosphere on ULF time scales.

4. Discussion and Conclusions

[28] Quantifying magnetohydrodynamic wave properties at geosynchronous orbit is important for radiation belt studies, because it is in the region where the energy coupling between ULF waves and relativistic electrons is greatest [*O'Brien et al.*, 2003]. In past decades, scientists have combined experimental and theoretical techniques to make significant progress in understanding the sources, propagation, and detailed characteristics of ULF waves. In contrast to

Table 1. Cubic Fit Coefficients for GOES ULF Wave Data on Various Solar Wind *Vx* and *Kp* Bins

V_x Bin					*Kp* Bin				
V_x Value (km/s)	C_3	C_2	C_1	C_0	*Kp* Value	C_3	C_2	C_1	C_0
				B_n Component					
300	−0.0053	0.1132	−0.9168	2.4390	0	−0.0060	0.1155	−0.8944	1.8851
400	−0.0045	0.1015	−0.8813	2.7306	1	−0.0059	0.1222	−0.9691	2.4074
500	−0.0021	0.0714	−0.7938	3.1036	2	−0.0035	0.0950	−0.9095	2.9455
600	0.0006	0.0314	−0.6154	3.2137	3	−0.0026	0.0791	−0.8249	3.3074
700	0.0001	0.0324	−0.5852	3.3172	4	−0.0017	0.0616	−0.7091	3.5532
800	0.0026	−0.0028	−0.4405	3.4999	5	−0.0007	0.0434	−0.6154	3.8350
				B_ϕ Component					
300	−0.0029	0.0543	−0.5626	1.6811	0	−0.0015	0.0356	−0.4836	1.3110
400	−0.0016	0.0401	−0.5165	1.8677	1	−0.0008	0.0303	−0.4918	1.5437
500	0.0003	0.0119	−0.3990	2.1236	2	−0.0016	0.0412	−0.5348	1.8943
600	0.0007	0.0050	−0.3579	2.3704	3	−0.0021	0.0493	−0.5651	2.4441
700	−0.0002	0.0157	−0.3712	2.6009	4	0.0005	0.0162	−0.4600	3.0542
800	0.0025	−0.0184	−0.2754	2.9708	5	0.0012	0.0067	−0.4285	3.4845
				B_n Component					
300	−0.0063	0.1185	−0.9183	2.2392	0	−0.0068	0.1236	−0.9290	1.8521
400	−0.0058	0.1146	−0.9189	2.5731	1	−0.0066	0.1252	−0.9664	2.2423
500	−0.0029	0.0738	−0.7513	2.8291	2	−0.0038	0.0906	−0.8517	2.6089
600	−0.0000	0.0337	−0.5930	2.9932	3	−0.0032	0.0793	−0.7836	2.9643
700	0.0008	0.0198	−0.5158	3.1171	4	−0.0024	0.0707	−0.7517	3.4505
800	0.0008	0.0153	−0.4830	3.4338	5	−0.0020	0.0622	−0.7023	3.8141

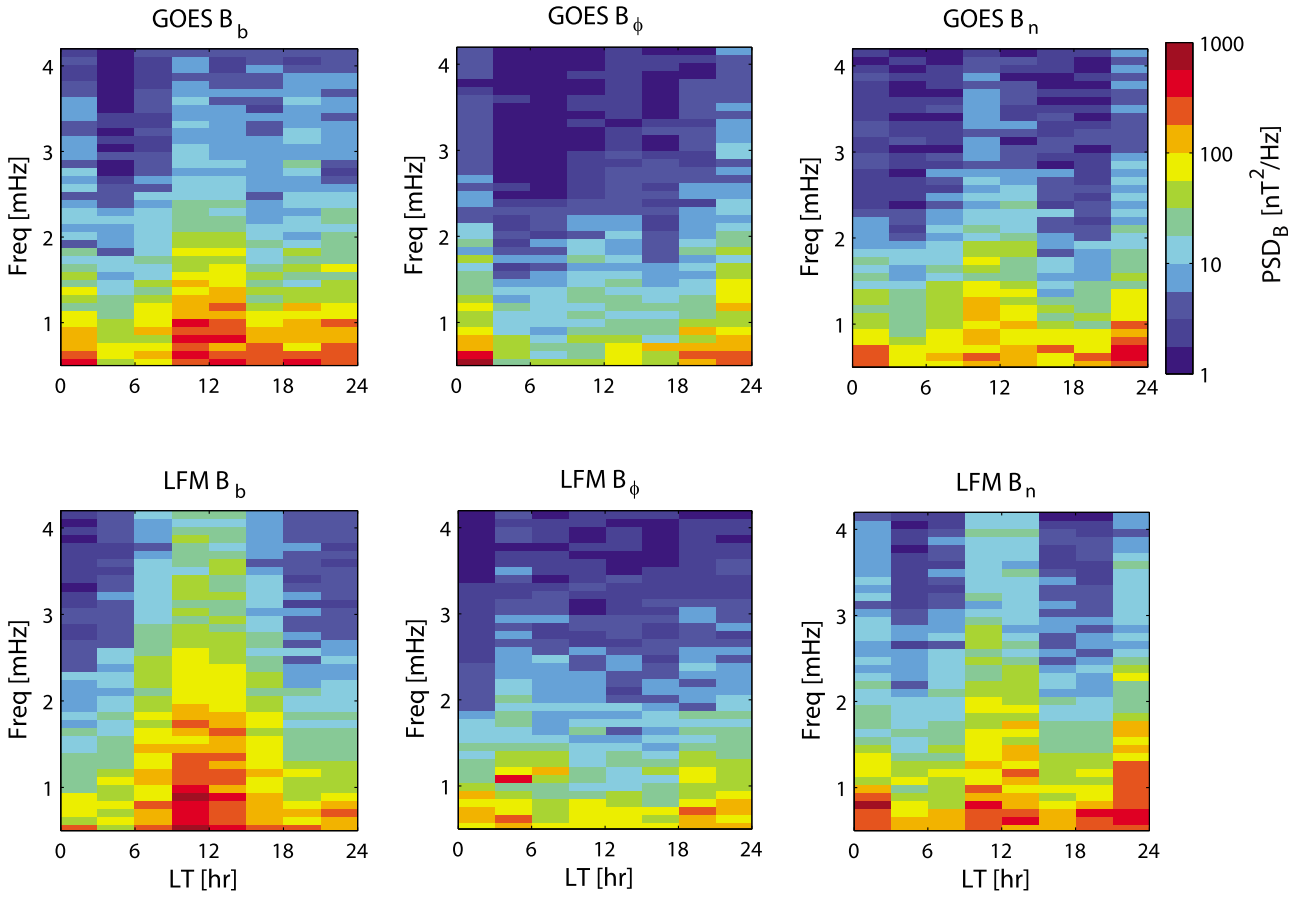

Figure 7. PSD comparisons of (top) GOES-8 data and (bottom) LFM code outputs at GOES-8 orbit in field-aligned coordinates ((left) B_b, (middle) B_ϕ and (right) B_n) for a 27 d interval. ULF wave power as a function of local time and frequency is shown on a colored logarithmic scale from 10^0 to 10^3 nT^2/Hz.

previous work, we do not study the nature of the waves, but rather we characterize the ULF wave power in observations and a global magnetospheric model in order to quantify the wave effects on the radiation belt electrons. We use power spectral density to characterize the ULF waves in the inner magnetosphere using magnetic field observations and global magnetospheric models. While the integrated wave power is known to be dominated by the lower-frequency bands, PSD reveals how the wave intensity as a function of frequency varies with location and controlling parameters. It is important for radiation belt studies to identify the wave power at specific frequencies that affect specific particle populations (e.g., the drift resonance frequency of a 1 MeV electron at geosynchronous orbit is ~1 mHz while a 5 MeV electron is resonant with ~5 mHz waves).

[29] Both the GOES wave statistical study and model wave predictions show compressional ULF wave power peaks at noon and midnight while the transverse components peak in the midnight sector. Such local time distributions are similar to the results of *Zhu and Kivelson* [1991] and *Takahashi and Ukhorskiy* [2007] for all field components. This similarity demonstrates that these independent studies using different data sets and PSD calculation methods reach similar conclusions. However, the local time distribution at geosynchronous orbit is different from that at other radial distances, as shown by *Zhu and Kivelson* [1991] and other studies. This suggests that the wave generation or propagation mechanisms are different for different regions in the magnetosphere. For example, at geosynchronous orbit, the majority of the ULF wave power at dayside is produced by solar wind pressure variations and wave power at nightside is from storms and substorms caused by interplanetary magnetic field fluctuations.

[30] Additionally, we quantify the GOES PSDs as functions of various controlling parameters to better understand how the magnetic field responds over short time scales during different conditions. The general increase of ULF wave power in the compressional, azimuthal and radial components varies similarly as the level of each parameter increases. ULF wave power increases at all local times as solar wind V_x and dynamic pressure variation increase, consistent with dynamic pressure variations growing with higher solar wind velocity and directly driving the magnetosphere at ULF wave frequencies. When IMF B_z is northward, wave activity is concentrated on the local dayside. Throughout IMF B_z southward intervals, the solar wind-magnetosphere coupling process creates stronger and broader perturbations as B_z becomes more negative, especially on the nightside. During intervals of large global disturbances, described by *Kp* and *Dst*, wave power increases at all local times and frequencies. On the other hand, wave distributions during substorm events, described best by the *AE* index, are strongest on the nightside as a consequence of localized tail field dipolarization.

[31] The formation of ULF waves in the magnetosphere is the combination of many physical processes. To find the geomagnetic index that best describes the ULF wave power at geosynchronous orbit, we compare the correlation coefficients between the integrated wave power of GOES data and the different parameters. The integrated wave powers are calculated from the PSD maps from Figure 3, 4, and 5. For each PSD map, we take an average of the local time PSD and integrate the spectral density over the frequency range (0.5 to 8.2 mHz) to obtain the integrated wave power value in units of nT^2. To compare the correlation between wave power and given parameters, we calculate Spearman's rank correlation coefficient. This measure of correlation describes the relation between two variables without making any assumption about the distribution of the variables. The correlation coefficients for solar wind V_x, dynamic pressure variations ΔP_d, IMF B_z, *Kp*, *Dst*, and *AE* are 1, 1, 0.6, 1, 0.94, and 1, respectively. The integrated wave power grows as the solar wind driver or geomagnetic activity increases with high correlation with all of the parameters. Comparing the three solar wind drivers, the coefficient value of IMF B_z is smaller than solar wind velocity and dynamic pressure variations, because IMF B_z has a less direct effect on geomagnetic field perturbation. Larger solar wind velocities generate Kelvin-Helmholtz waves on the flanks and higher dynamic pressure variations create more magnetospheric fluctuations at ULF frequencies.

[32] Finally, we examine the ULF wave predictions from a global magnetospheric MHD code for the first time. Since the waves are a second-order quantity produced by the model, we have limited expectations of the accuracy of the code in predicting detailed wave properties compared to GOES data on an event to event basis. However, we may reasonably expect the modeled wave statistical properties to agree with observations. The LFM code predicts wave properties well in a statistical sense in comparison to GOES data under typical solar wind conditions for 27 days of a nonstorm interval. Although the LFM code does not predict magnetic field configurations perfectly due to the lack of a sufficient current system in the inner magnetosphere, the ULF wave predictions at geosynchronous orbit are surprisingly good.

[33] In summary, we demonstrate new ways to characterize and study ULF waves in the inner magnetosphere that are critical for controlling radiation belt electron dynamics. A statistical study of GOES magnetic field data provides a characterization of ULF wave spectra at geosynchronous orbit during different solar wind conditions and levels of geomagnetic activity. Based on these characterizations, we describe the wave local time distribution and amplitude as a function of given solar wind conditions and geomagnetic activity. Exploring wave properties in a magnetospheric model also shows the strengths and limitations of the physics-based model in predicting field fluctuations on a global scale. The MHD simulation reproduces the ULF waves remarkably well. Quantifying ULF waves using data and model output helps to better understand the physical processes of the inner magnetosphere and also represents a significant contribution to radiation belt research. We have demonstrated that the LFM code is capable of reproducing magnetospheric ULF waves through solving the MHD equations globally even when lacking some known magnetospheric physics in the code.

[34] In this paper, we constructed the most comprehensive observational ULF wave study at geosynchronous orbit that can be used for outer zone electron studies. The statistical study results, local time distributions of ULF waves and wave power as functions of solar wind conditions and geomagnetic activity levels, are important and essential elements needed to better understand wave induced particle diffusion in the magnetosphere. In addition, we made the first direct comparison of wave power generated by global magnetospheric models with observations. The LFM code produces reasonable ULF wave power during typical conditions which is a significant contribution to the radiation belt studies. This

work fills in a long-standing gap by identifying a wave field model that provides global, time-dependent ULF wave fields in the magnetosphere. Based on this work, we perform radial transport calculation of radiation belt electrons using the LFM code in the companion paper [*Huang et al.*, 2010].

[35] **Acknowledgments.** We thank M. K. Hudson and J. G. Lyon for helpful discussions and suggestions. We acknowledge the WDC for Geomagnetism, Kyoto University, Japan for the geomagnetic indices, and CDAWeb for GOES and Wind data. This material is based upon work supported by Center for Integrated Space Weather Modeling (CISM) funded by the Science and Technology Centers Program of the National Science Foundation under agreement ATM-0120950 and by the NASA Radiation Belt Storm Probes (RBSP) mission funded under JHU/APL subcontract 923497 of prime NASA contract NAS5-01072.

[36] Zuyin Pu thanks Wenlong Liu and another reviewer for their assistance in evaluating this paper.

References

Anderson, B. J. (1994), An overview of spacecraft observations of 10s to 600s period magnetic pulsations, in *Solar Wind Sources of Magnetospheric Ultra-Low-Frequency Waves*, *Geophys. Monogr. Ser.*, vol. 81, edited by M. Engebretson, K. Takahashi, and M. Scholer, p. 25, AGU, Washington, D. C.

Anderson, B. J., M. J. Engebretson, S. P. Rounds, L. J. Zanetti, and T. A. Potemra (1990), A statistical study of Pc 3-5 pulsations observed by the AMPTE/CCE magnetic fields experiment, 1. Occurrence distributions, *J. Geophys. Res.*, *95*, 10,495–10,523, doi:10.1029/JA095iA07p10495.

Brautigam, D. H., and J. M. Albert (2000), Radial diffusion analysis of outer radiation belt electrons during the October 9, 1990, magnetic storm, *J. Geophys. Res.*, *105*, 291–309, doi:10.1029/1999JA900344.

Brautigam, D. H., G. P. Ginet, J. M. Albert, J. R. Wygant, D. E. Rowland, A. Ling, and J. Bass (2005), CRRES electric field power spectra and radial diffusion coefficients, *J. Geophys. Res.*, *110*, A02214, doi:10.1029/2004JA010612.

Claudepierre, S., S. Elkington, and M. Wiltberger (2008), Solar wind driving of magnetospheric ULF waves: Pulsations driven by velocity shear at the magnetopause, *J. Geophys. Res.*, *113*, A05218, doi:10.1029/2007JA012890.

Dungey, J. W. (1954), Electrodynamics of the outer atmosphere, Rep. 69, Ions. Res. Lab., Pa. Sate Univ., University Park, Pa.

Elkington, S. R., M. K. Hudson, and A. A. Chan (1999), Acceleration of relativistic electrons via drift-resonant interaction with toroidal-mode Pc-5 ULF oscillations, *Geophys. Res. Lett.*, *26*, 3273–3276, doi:10.1029/1999GL003659.

Elkington, S. R., M. K. Hudson, and A. A. Chan (2003), Resonant acceleration and diffusion of outer zone electrons in an asymmetric geomagnetic field, *J. Geophys. Res.*, *108*(A3), 1116, doi:10.1029/2001JA009202.

Elkington, S. R., M. Wiltberger, A. A. Chan, and D. N. Baker (2004), Physical models of the geospace radiation environment, *J. Atmos. Sol. Terr. Phys.*, *66*, 1371–1387.

Higuchi, T., and S. Kokubun (1988), Waveform and polarization of compressional Pc-5 waves at geosynchronous orbit, *J. Geophys. Res.*, *93*, 14,433–14,443.

Huang, C.-L., H. E. Spence, J. G. Lyon, F. R. Toffoletto, H. J. Singer, and S. Sazykin (2006), Storm-time configuration of the inner magnetosphere: Lyon-Fedder-Mobarry MHD code, Tsyganenko model, and GOES observations, *J. Geophys. Res.*, *111*, A11S16, doi:10.1029/2006JA011626.

Huang, C.-L., H. E. Spence, M. K. Hudson, and S. R. Elkington (2010), Modeling radiation belt radial diffusion in ULF wave fields: 2. Estimating rates of radial diffusion using combined MHD and particle codes, *J. Geophys. Res.*, *115*, A06216, doi:10.1029/2009JA014918.

Hudson, M. K., S. R. Elkington, J. G. Lyon, C. C. Goodrich, and T. J. Rosenberg (1999), Simulation of radiation belt dynamics driven by solar wind variations, in *Sun-Earth Plasma Connections*, *Geophys. Monogr. Ser.*, vol. 109, edited by J. L. Burch, R. L. Carovillano, and S. K. Antiochos, p. 171–182, AGU, Washington, D. C.

Hudson, M. K., S. R. Elkington, J. G. Lyon, and C. C. Goodrich (2000), Increase in the relativistic electron flux in the inner magnetosphere: ULF wave mode structure, *Adv. Space Res.*, *25*, 2327–2337.

Hudson, M. K., R. E. Denton, M. R. Lessard, E. G. Miftakhova, and R. R. Anderson (2004), A study of Pc-5 ULF oscillations, *Ann. Geophys.*, *22*, 289–302.

Hughes, W. J. (1994), Magnetospheric ULF waves: A tutorial with a historical perspective, in *Solar Wind Sources of Magnetospheric Ultra-Low-Frequency Waves*, *Geophys. Monogr. Ser.*, vol. 81, edited by M. Engebretson, K. Takahashi, and M. Scholer, pp. 1–11, AGU, Washington, D. C.

Hughes, W. J., D. J. Southwood, B. Mauk, R. L. McPherron, and J. N. Barfield (1978), Alfén waves generated by an inverted plasma energy distribution, *Nature*, *275*, 43–45.

Kepko, L., H. E. Spence, and H. J. Singer (2002), ULF waves in the solar wind as direct drivers of magnetospheric pulsations, *Geophys. Res. Lett.*, *29*(8), 1197, doi:10.1029/2001GL014405.

Lyon, J. G., J. A. Fedder, and C. M. Mobarry (2004), The Lyon-Fedder-Mobarry (LFM) global MHD magnetospheric simulation code, *J. Atmos. Sol. Terr. Phys.*, *66*, 1333–1350.

Mathie, R. A., and I. R. Mann (2001), On the solar wind control of Pc5 ULF pulsation power at mid-latitudes: Implications for MeV electron acceleration in the outer radiation belt, *J. Geophys. Res.*, *106*, 29,783–29,796, doi:10.1029/2001JA000002.

O'Brien, T. P., R. L. McPherron, D. Sornette, G. D. Reeves, R. Friedel, and H. J. Singer (2001), Which magnetic storms produce relativistic electrons at geosynchronous orbit?, *J. Geophys. Res.*, *106*, 15,553–15,544, doi:10.1029/2001JA000052.

O'Brien, T. P., K. R. Lorentzen, I. R. Mann, N. P. Meredith, J. B. Blake, J. F. Fennell, M. D. Looper, D. K. Milling, and R. R. Anderson (2003), Energization of relativistic electrons in the presence of ULF power and MeV microbursts: Evidence for dual ULF and VLF acceleration, *J. Geophys. Res.*, *108*(A8), 1329, doi:10.1029/2002JA009784.

Perry, K. L., M. K. Hudson, and S. R. Elkington (2006), Correction to "Incorporating spectral characteristics of Pc5 waves into three-dimensional radiation belt modeling and the diffusion of relativistic electrons", *J. Geophys. Res.*, *111*, A11228, doi:10.1029/2006JA012040.

Pu, Z., and M. G. Kivelson (1983), Kelvin-Helmholtz instability at the magnetopause: Energy flux into the magnetosphere, *J. Geophys. Res.*, *88*, 853–861, doi:10.1029/JA088iA02p00853.

Rostoker, G., S. Skone, and D. N. Baker (1998), On the origin of relativistic electrons in the magnetosphere associated with some geomagnetic storms, *Geophys. Res. Lett.*, *25*, 3701–3704, doi:10.1029/98GL02801.

Singer, H., and M. Kivelson (1979), The latitudinal structure of Pc5 waves in space: Magnetic and electric field observations, *J. Geophys. Res.*, *84*, 7213–7222.

Southwood, D. J. (1977), The role of hot plasma in magnetospheric convection, *J. Geophys. Res.*, *82*, 5512–5520.

Southwood, D. J., and W. J. Hughes (1983), Theory of hydromagnetic waves in the magnetosphere, *Space Sci. Rev.*, *35*, 301–366.

Takahashi, K., and B. J. Anderson (1992), Distribution of ULF energy ($f <$ 80 mHz) in the inner magnetosphere: A statistical analysis of AMPTE CCE magnetic field data, *J. Geophys. Res.*, *97*, 10,751–10,773, doi:10.1029/92JA00328.

Takahashi, K., and A. Y. Ukhorskiy (2007), Solar wind control of Pc5 pulsation power at geosynchronous orbit, *J. Geophys. Res.*, *112*, A11205, doi:10.1029/2007JA012483.

Takahashi, K., P. J. Chi, R. E. Denton, and R. L. Lysak (Eds.) (2006), *Magnetospheric ULF Waves: Synthesis and New Directions*, *Geophys. Monogr. Ser.*, vol. 169, AGU, Washington, D. C.

Wilson, M. E., T. K. Yeoman, L. J. Baddeley, and B. J. Kellet (2006), A statistical investigation of the invariant latitude dependence of unstable magnetospheric ion populations in relation to high m ULF wave generation, *Ann. Geophys.*, *24*, 3027–3040.

Zhu, X., and M. G. Kivelson (1991), Compressional ULF waves in the outer magnetosphere, 1. Statistical study, *J. Geophys. Res.*, *96*, 19,451–19,467, doi:10.1029/91JA01860.

C.-L. Huang, W. J. Hughes, and H. E. Spence, Center for Space Physics, Boston University, 725 Commonwealth Ave., Boston, MA 02215, USA. (hcl@bu.edu)

H. J. Singer, Space Weather Prediction Center, NOAA, 325 Broadway, Boulder, CO 80305, USA.